Accurate nucleon electromagnetic form factors from dispersively improved chiral effective field theory

J.M. Alarcón *, C. Weiss

Theory Center, Jefferson Lab, Newport News, VA 23606, USA

A B S T R A C T

We present a theoretical parametrization of the nucleon electromagnetic form factors (FFs) based on a combination of chiral effective field theory and dispersion analysis. The isovector spectral functions on the two-pion cut are computed using elastic unitarity, chiral pion–nucleon amplitudes, and timelike pion FF data. Higher-mass isovector and isoscalar t-channel states are described by effective poles, whose strength is fixed by sum rules (charges, radii). Excellent agreement with the spacelike proton and neutron FF data is achieved up to $Q^2 \sim 1$ GeV^2. Our parametrization provides proper analyticity and theoretical uncertainty estimates and can be used for low-Q^2 FF studies and proton radius extraction.

© 2018 The Authors. Published by Elsevier B.V. This is an open access article under the CC BY license (http://creativecommons.org/licenses/by/4.0/). Funded by SCOAP³.

1. Introduction

The electromagnetic form factors (EM FFs) parametrize the transition matrix element of the EM current between nucleon states and represent basic characteristics of nucleon structure. The FFs at spacelike momentum transfers $Q^2 \lesssim 1$ GeV^2 have been measured in a series of elastic electron scattering experiments [1–3], most recently at the Mainz Microtron (MAMI) [4–6] and at Jefferson Lab [7–9]. The derivative of the proton electric FF at $Q^2 = 0$ (charge radius) is also determined with high precision in atomic physics experiments. Discrepancies between results obtained with different methods have raised interesting questions concerning the precise value of the proton charge radius and the $Q^2 \to 0$ extrapolation of the elastic scattering data [10–12]. Besides their importance for nucleon structure, the EM FFs are needed as an input in other areas of study, such as precision measurements of quantities used to test the Standard Model.

The experiments and applications require a theoretical description of the FFs that covers a broad range $Q^2 \sim$ few GeV^2 and controls the behavior in the $Q^2 \to 0$ limit (higher derivatives). This can be accomplished using the framework of dispersion theory, which incorporates the analytic properties of the FFs in the momentum transfer. Dispersive parametrizations of the nucleon FFs have been constructed using empirical spectral functions, determined by amplitude analysis techniques and fits to the FF data

[13–16]. It would be desirable to have a dispersive parametrization that is based on first-principles dynamical calculations and permits theoretical uncertainty estimates.

In recent work we developed a method for computing the spectral functions of nucleon FFs on the two-pion cut using a combination of chiral effective field theory (χEFT) and amplitude analysis (dispersively improved χEFT, or DIχEFT) [17,18]. The spectral functions are constructed using the elastic unitarity condition. The N/D method is used to separate the $\pi\pi$ rescattering effects (contained in the pion timelike FF) from the coupling of the $\pi\pi$ system to the nucleon (calculable in χEFT with good convergence). The method permits computation of the two-pion spectral functions up to masses ~ 1 GeV^2 with controlled accuracy. In Ref. [18] the computed spectral functions in LO, NLO, and partial N2LO, accuracy were used to study the FFs at low Q^2 (<0.5 GeV^2 for G_E, <0.2 GeV^2 for G_M) and their derivatives.

In this letter we use DIχEFT to calculate the nucleon FFs up to $Q^2 \sim 1$ GeV^2 (and higher) and construct a dispersive parametrization of the FFs with theoretical uncertainty estimates. This is achieved by extending our previous calculations in two aspects: (a) We partially include N2LO chiral loop corrections in the isovector magnetic spectral function, by parametrizing them in a form similar to the N2LO corrections in the electric case. This brings the calculation of electric and magnetic isovector FFs up to the same order. (b) We account for higher-mass t-channel states in the spectral functions (isovector and isoscalar) by parametrizing them through effective poles, whose strength is determined by sum rules (charges, magnetic moments, radii). This allows us to extend the

---

dispersion integrals to higher masses and compute the spacelike FFs up to higher Q^2. We obtain an excellent description of G_E and G_M up to $Q^2 \sim 2$ GeV^2 with controlled theoretical accuracy. Our results represent theoretical predictions in the sense that no fits are performed, and no empirical information from the FFs other than the radii is used in determining the parameters. In the following we describe the calculation and results and discuss potential applications of our FF parametrization.

2. Method

The FFs are analytic functions of the invariant momentum transfer $t \equiv -Q^2$ and satisfy dispersion relations

$$G_i^{p,n}(t) = \frac{1}{\pi} \int_{t_{\text{thr}}}^{\infty} dt' \frac{\text{Im}\, G_i^{p,n}(t')}{t' - t - i0} \quad (i = E, M). \tag{1}$$

They allow one to reconstruct the spacelike FFs from the spectral functions $\text{Im}\, G_i^{p,n}(t')$ on the cut at $t' > t_{\text{thr}}$. For theoretical analysis one uses the isovector and isoscalar combinations, $G_i^{V,S} \equiv \frac{1}{2}(G_i^p \mp G_i^n)$ ($i = E, M$). In the isovector FF the lowest singularity is the two-pion cut with $t_{\text{thr}} = 4M_\pi^2$. The spectral functions on the two-pion cut can be obtained from the elastic unitarity conditions, which in the N/D representation take the form [13,19,20]

$$\text{Im}\, G_E^V(t')[\pi\pi] = \frac{k_{\text{cm}}^3}{m_N \sqrt{t'}} J_+^1(t') |F_\pi(t')|^2, \tag{2}$$

$$\text{Im}\, G_M^V(t')[\pi\pi] = \frac{k_{\text{cm}}^3}{\sqrt{2t'}} J_-^1(t') |F_\pi(t')|^2, \tag{3}$$

where $k_{\text{cm}} = \sqrt{t'/4 - M_\pi^2}$ is the center-of-mass momentum of the $\pi\pi$ system in the t-channel. Here $J_\pm^1(t') \equiv f_\pm^1(t')/F_\pi(t')$ are the ratios of the $\pi\pi \to N\bar{N}$ partial-wave amplitudes and the timelike pion FF, which are real for $t' > 4M_\pi^2$ and free of $\pi\pi$ rescattering effects. These functions can be computed in χEFT with good convergence [17,18]. $|F_\pi(t')|^2$ is the squared modulus of the timelike pion FF, which contains the $\pi\pi$ rescattering effects and the ρ meson resonance. This function is measured in $e^+e^- \to \pi^+\pi^-$ exclusive annihilation experiments with high precision and can be taken from a parametrization of the data; see Ref. [21] for a review. Because the $\pi\pi$ state practically exhausts the e^+e^- annihilation cross section at $t' \lesssim 1$ GeV^2, the elastic unitarity relations Eqs. (2) and (3) are assumed to be valid up to $t' = 1$ GeV^2.

The calculation of the $J_\pm^1$ functions in relativistic χEFT is described in Ref. [18]. At LO they are given by the N and Δ Born terms in the $\pi\pi \to N\bar{N}$ amplitudes and the Weinberg–Tomozawa term. At NLO corrections arise at tree-level from an NLO $\pi\pi NN$ contact term in the chiral Lagrangian. At N2LO pion loop corrections appear, and the structure becomes considerably more complex. In Ref. [18] we estimated the N2LO corrections to J_+^1 by assuming that the full N2LO result has the same structure as the tree-level N2LO result, in which the dominant contribution is the term proportional to $d_1 + d_2$. No such estimate was performed for J_-^1, since its N2LO corrections arise entirely from loops. In order to extend the reach of our calculation we now want to estimate J_+^1 and J_-^1 at the same level. This becomes possible with a generalization of our previous arguments. Inspecting the structure of the N2LO loop corrections in the $\pi N \to \pi N$ amplitude, we find that the dominant t-channel correction can be parametrized as

$$A^-[\text{N2LO loop}] = 0, \qquad B^-[\text{N2LO loop}] = \lambda\, t/f_\pi^2, \tag{4}$$

where A and B are the invariant amplitudes [22]. In this form the N2LO loop result in J_-^1 has the same structure as a tree-level correction arising from contact terms, and the parameter λ can be determined in the same way as in our previous estimate for J_+^1.

In order to extend the isovector spectral integrals to masses $t' > 1$ GeV^2 we need to parametrize the isovector spectral function beyond the two-pion cut. The e^+e^- exclusive annihilation data show that the isovector cross section above $t' \sim 1$ GeV^2 is overwhelmingly in the 4π channel and peaks at $t' \approx 2.3$ GeV^2 [21]. (Incidentally, this value coincides with the squared mass of the ρ' resonance observed in the $\pi\pi$ channel.) It is reasonable to assume that the strength distribution in the nucleon spectral function follows a similar pattern. The simplest way to parametrize the high-mass contribution to the isovector spectral function is by a single effective pole,

$$\text{Im}\, G_{E,M}^V(t')[\text{high-mass}] = \pi a_{E,M}^{(1)} \delta(t' - M_1^2), \tag{5}$$

where we choose $M_1^2 = M_{\rho'}^2 = 2.1$ GeV^2. The total isovector spectral function is given by the sum of the $\pi\pi$ cut (calculated in DIχEFT) and the high-mass part (parametrized by the effective pole),

$$\text{Im}\, G_{E,M}^V = \text{Im}\, G_{E,M}^V[\pi\pi] + \text{Im}\, G_{E,M}^V[\text{high-mass}]. \tag{6}$$

We then determine the parameters of the N2LO contributions in $G_{E,M}^V[\pi\pi]$ and the strength of the effective pole in $G_{E,M}^V[\text{high-mass}]$ by imposing the sum rules for the isovector charge and magnetic moment, and for the electric and magnetic radii (here $t_{\text{thr}} = 4M_\pi^2$):

$$\frac{1}{\pi} \int_{t_{\text{thr}}}^{\infty} dt' \frac{\text{Im}\, G_E^V(t')}{t'} = \frac{1}{2}, \tag{7}$$

$$\frac{1}{\pi} \int_{t_{\text{thr}}}^{\infty} dt' \frac{\text{Im}\, G_M^V(t')}{t'} = \frac{1}{2}(\mu^p - \mu^n), \tag{8}$$

$$\frac{6}{\pi} \int_{t_{\text{thr}}}^{\infty} dt' \frac{\text{Im}\, G_E^V(t')}{t'^2} = \langle r^2 \rangle_E^V \equiv \frac{1}{2}[\langle r^2 \rangle_E^p - \langle r^2 \rangle_E^n], \tag{9}$$

$$\frac{6}{\pi} \int_{t_{\text{thr}}}^{\infty} dt' \frac{\text{Im}\, G_M^V(t')}{t'^2} = \langle r^2 \rangle_M^V \equiv \frac{1}{2}[\mu^p \langle r^2 \rangle_M^p - \mu^n \langle r^2 \rangle_M^n]. \tag{10}$$

Since the charge and magnetic moment are known precisely, the unknown parameters are essentially determined in terms of the isovector charge and magnetic radii, which can be allowed to vary over a reasonable range (see below). This makes our parametrization particularly convenient for applications where the nucleon radii are regarded as basic parameters or extracted from data.

In the isoscalar FF the lowest singularity is the 3-pion cut ($t_{\text{thr}} = 9M_\pi^2$). The strength at $t' < 1$ GeV^2 is overwhelmingly concentrated in the ω resonance, which we describe by a zero-width pole. At $t' \gtrsim 1$ GeV^2 the $K\bar{K}$ and other channels open up. The exclusive e^+e^- annihilation data show that the strength at $t' \sim 1$ GeV^2 is concentrated in the ϕ resonance [21]. We therefore parametrize the high-mass isoscalar strength by an effective pole at the ϕ mass. Altogether, our parametrization of the isoscalar spectral function is

$$\text{Im}\, G_{E,M}^S(t') = \pi a_{E,M}^\omega \delta(t' - M_\omega^2) + \pi a_{E,M}^\phi \delta(t' - M_\phi^2). \tag{11}$$

Table 1

Parameters of the effective poles describing the high-mass isovector spectral function, Eq. (5), and the isoscalar spectral function, Eq. (11), as determined by the sum rule Eqs. (7)–(10) and the corresponding isoscalar sum rule.

$a_E^{(1)}$	$(-0.853, -0.58)$
$a_M^{(1)}$	$(-2.601, -1.194)$
a_E^{ω}	$(0.722, 0.840)$
a_M^{ω}	$(0.613, 0.898)$
a_E^{ϕ}	$(-0.905, -0.705)$
a_M^{ϕ}	$(-1.064, -0.581)$

The strength of the ω and high-mass (ϕ) poles are fixed by imposing the sum rules for the isoscalar charges and radii, i.e., the analog of Eqs. (7)–(10) with $V \to S$ and $(p - n) \to (p + n)$.

In fixing the isovector and isoscalar spectral function parameters through the sum rules Eqs. (7)–(10) and their isoscalar analog, we use the Particle Data Group (PDG) values of the proton and neutron charge radii and their uncertainties [23]. To the isovector charge radius we assign an uncertainty larger than the PDG range in order to cover also the results of a dispersive calculation [24]. For the proton and neutron magnetic radii we use the results of Refs. [16,25], which are compatible with the PDG values in the neutron case. The empirical variation of the radii generates a range of the parameters, which then produces the uncertainty bands in our predictions. The resulting parameters are summarized in Table 1. The uncertainty induced by the empirical pion timelike FF in the isovector calculation using Eqs. (2) and (3) is small and can be neglected.

In the present calculation we parametrize the high-mass states in the spectral functions by a single effective pole, whose strength can be fixed by the sum rules. The approximation is justified as long as we restrict ourselves to the spacelike FFs at moderate momentum transfers $|t| \sim 1\,\mathrm{GeV}^2$. We can demonstrate this explicitly for the isovector FF, using a technique described in Ref. [13]. We take the difference of the empirical spacelike FF and the finite dispersive integral over the $\pi\pi$ cut up to $t_{max} = 1\,\mathrm{GeV}^2$,

$$\Delta_E(t) \equiv G_E^V(t)[\mathrm{emp}] - \frac{1}{\pi} \int_{t_{\mathrm{thr}}}^{t_{\max}} dt' \frac{\mathrm{Im}\,G_E^V(t')[\pi\pi]}{t' - t - i0}. \quad (12)$$

This quantity represents the high-mass part of the dispersive integral, which is to be approximated by the dispersive integral with the effective pole, $a_E^{(1)}/(t - M_1^2)$. Plotting $1/\Delta_E(t)$ at $t < 0$ (see Fig. 1) one sees that the dependence on t is approximately linear, and that the single-pole form provides an adequate description up to $|t| < 2\,\mathrm{GeV}^2$. Note that this is achieved with the pole parameters fixed by the sum rules Eqs. (7)–(10), and that we do not perform a fit of the spacelike FF data in Fig. 1.

The nucleon FFs obey superconvergence relations

$$\int_{t_{\mathrm{thr}}}^{\infty} dt' \,\mathrm{Im}\,G_i^{V,S}(t') = 0 \quad (i = E, M), \quad (13)$$

which guarantee the absence of powers t^{-1} in the asymptotic behavior for $|t| \to \infty$. In the present calculation we focus on the FFs at limited spacelike momenta $|t| \lesssim 1\,\mathrm{GeV}^2$ and are not concerned with the asymptotic behavior. The relation Eq. (13) could easily be implemented in our approach by parametrizing the high-mass spectral density in a more flexible form; however, this would require fitting the spacelike FF data in order to determine the parameters, which is not our intention here.
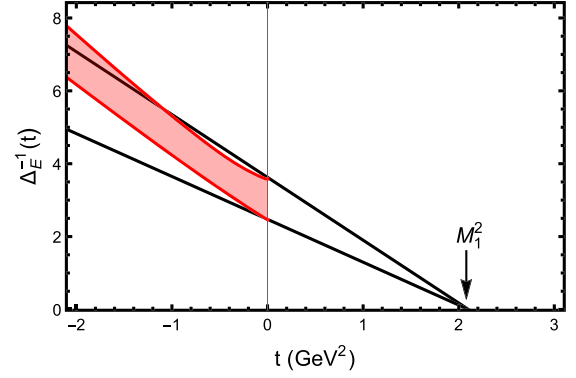

Fig. 1. Red band: Inverse difference $1/\Delta_E(t)$, Eq. (12). Black lines: Inverse of the dispersive integral with the single-pole parametrization Eq. (5) and the parameters listed in Table 1. (For interpretation of the colors in the figure(s), the reader is referred to the web version of this article.)
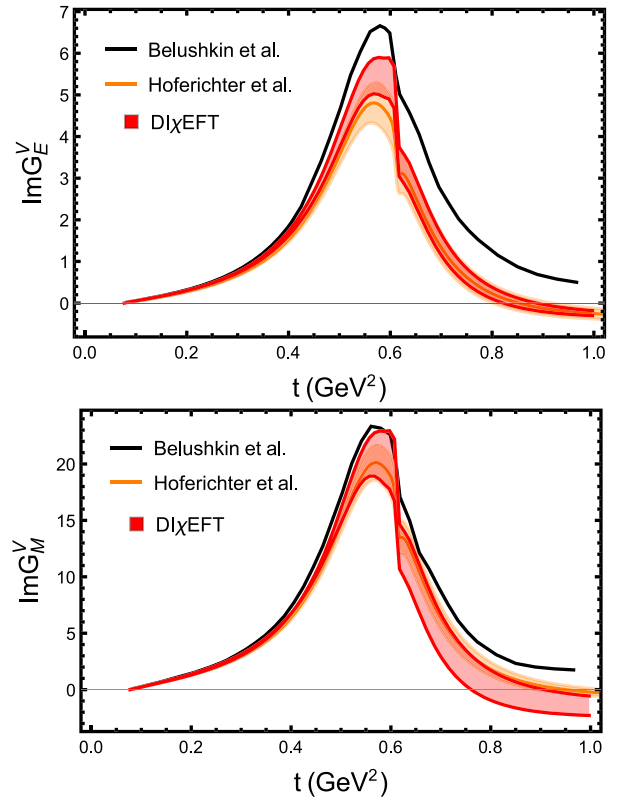
Fig. 2. Red bands: Isovector spectral functions on the two-pion cut calculated in our approach and their theoretical uncertainty. Orange bands: Spectral functions obtained in Roy–Steiner analysis of Ref. [24]. Black line: Spectral functions of Ref. [26].

3. Results

The spectral functions are the primary quantities calculated in our approach. The results for the isovector spectral function on the two-pion cut, Eqs. (2) and (3), are shown in Fig. 2. The bands show the total uncertainty of our calculation, resulting from the uncertainty of the low-energy constants in the χEFT calculation and the empirical uncertainty of the nucleon radii used to fix the parameters (see above). Compared to Ref. [18] the electric and magnetic spectral functions are now calculated at the same order (LO + NLO + partial N2LO). Both spectral functions now show a trend to negative values above the ρ peak. Our results agree overall very well with those obtained in an analysis of πN scattering data using Roy–Steiner equations [24]; only in the ρ peak our $\mathrm{Im}\,G_E^V$ is
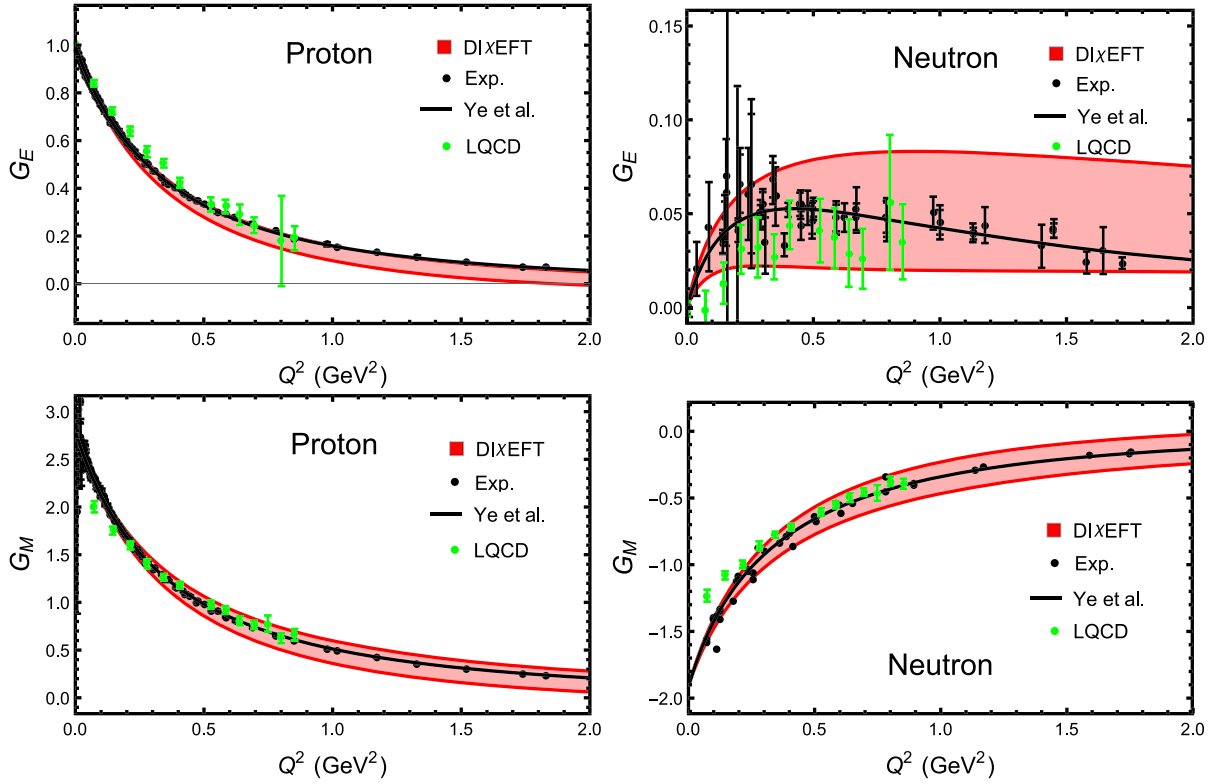
Fig. 3. Red bands: Proton and neutron EM FFs calculated in our approach and their theoretical uncertainties, as obtained from the variation of the nucleon radii (see text). Solid black: Empirical FF parametrization of Ref. [3]. Black dots: Data of the MAMI A1 experiment [4,5]. Green dots: Lattice QCD results from Ref. [27].

Table 2
FF moments obtained from the dispersive integral Eq. (14) with the DIχEFT spectral functions (LO + NLO + partial N2LO).

Moment	G_E^p	G_E^n	G_M^p	G_M^n
$\langle r^2 \rangle$ (fm^2)*	(0.701, 0.768)	(−0.079, −0.146)	(0.689, 0.765)	(0.713, 0.813)
$\langle r^4 \rangle$ (fm^4)	(1.473, 1.602)	(−0.635, −0.506)	(1.676, 1.782)	(2.045, 2.042)
$\langle r^6 \rangle$ (fm^6)	(8.519, 8.962)	(−6.110, −5.667)	(11.525, 11.579)	(15.231, 15.645)
$\langle r^8 \rangle$ (10^2 fm^8)	(1.269, 1.296)	(−1.159, −1.131)	(1.834, 1.882)	(2.597, 2.691)
$\langle r^{10} \rangle$ (10^3 fm^{10})	(3.933, 3.965)	(−3.866, −3.834)	(5.707, 5.905)	(8.274, 8.581)
$\langle r^{12} \rangle$ (10^5 fm^{12})	(2.041, 2.049)	(−2.039, −2.031)	(2.903, 3.004)	(4.233, 4.382)
$\langle r^{14} \rangle$ (10^7 fm^{14})	(1.557, 1.561)	(−1.559, −1.556)	(2.158, 2.230)	(3.150, 3.255)
$\langle r^{16} \rangle$ (10^9 fm^{16})	(1.624, 1.626)	(−1.626, −1.624)	(2.191, 2.260)	(3.198, 3.299)
$\langle r^{18} \rangle$ (10^{11} fm^{18})	(2.210, 2.212)	(−2.212, −2.210)	(2.905, 2.991)	(4.241, 4.367)
$\langle r^{20} \rangle$ (10^{13} fm^{20})	(3.796, 3.799)	(−3.799, −3.796)	(4.866, 5.006)	(7.105, 7.308)

*The $\langle r^2 \rangle$ moments are input values (see text).

∼15% larger. Our uncertainties are comparable to those of the Roy–Steiner analysis. Also shown in Fig. 2 are the empirical spectral functions of Ref. [26].

The spacelike EM FFs calculated with the dispersion integrals Eq. (1) are shown in Fig. 3. The proton and neutron FFs were obtained as $G_i^{p,n} = G_i^S \pm G_i^V$ ($i = E, M$). Contrary to Ref. [18] we now do not perform any subtractions and calculate the dispersive integral without a cutoff in t', as the high-mass parts of the spectral functions are now parametrized consistently through the effective poles. Our results show excellent agreement with the recent FF parametrization of Ref. [3] for all momentum transfers $Q^2 \lesssim$ 1 GeV^2, and even up ∼2 GeV^2, which is remarkable in view of our simple parametrization of the high-mass spectral functions. Note that G_E^n involves substantial cancellations between the isovector and isoscalar components, so that its relative uncertainties are larger than that of the other FFs.

The higher derivatives of the FFs (moments) are needed in the extraction of the proton radius from experimental data. In our dispersive approach they are evaluated as

$$\frac{\langle r^{2n} \rangle_i}{(2n+1)!} = \frac{1}{\pi} \int\limits_{t_{\text{thr}}}^{\infty} dt' \frac{\text{Im}\, G_i(t')}{t'^{n+1}} \quad (i = E, M); \tag{14}$$

see Ref. [18] for details. The moments obtained with our spectral functions are summarized in Table 2. Compared to the results quoted in Ref. [18] the isovector LO and NLO parts are exactly the same; the only changes are the estimated partial N2LO contributions and the added isovector high-mass contribution. The isoscalar part is the same as in Ref. [18]; only the couplings have now been determined through the charge and radius sum rules. Our new moments have smaller uncertainty than those of Ref. [18]. They confirm the "unnatural size" of the higher moments (compared to the dipole expectation) observed in Ref. [18].

4. Discussion

DIχEFT enables first-principles dynamical calculations of the isovector two-pion spectral functions with controlled uncertainties and gives results in good agreement with empirical amplitude analysis. Together with a minimal effective pole parametrization of the high-mass isovector and isoscalar states, the method provides an accurate dispersive description of the nucleon FFs up to momentum transfers $|t| \sim 1$ GeV^2 and above. The method is predictive in the sense that the dynamical input is provided by χEFT (with higher-order terms constrained by the nucleon radii) and e^+e^- annihilation data, and no fitting of nucleon FFs at $|t| \neq 0$ is performed. The calculation fixes the behavior of the FFs at $|t| > 0$ in terms of the radii, and it is possible to relate the uncertainties of one with the other. We note that purely empirical approaches cannot unambiguously predict the behavior of the FFs at finite $|t|$ in terms of the radii, or, conversely, extract the values of the radii from the finite-t data; see Ref. [28] and references therein for a detailed discussion. The new dynamical method therefore represents major progress in the theory of nucleon FFs at low momentum transfers.

Our results provide a FF parametrization with proper analyticity in t. It implements the correct position of the leading singularity on the physical sheet (two-pion threshold at $t_{\mathrm{thr}} = 4M_\pi^2$) and the basic distribution of strength on the principal cut (spectral function), which contains the essential information about dynamics. The parametrization can be used for theoretical or empirical studies in which analyticity is essential: (a) Determination of the peripheral charge and magnetization densities in the nucleon [29]; (b) extraction of the proton charge radius from ep elastic scattering data; (c) calculation of two-photon-exchange corrections in ep elastic scattering.

Acknowledgements

References

[1] C.F. Perdrisat, V. Punjabi, M. Vanderhaeghen, Prog. Part. Nucl. Phys. 59 (2007) 694, https://doi.org/10.1016/j.ppnp.2007.05.001.

[2] V. Punjabi, et al., Eur. Phys. J. A 51 (2015) 79, https://doi.org/10.1140/epja/i2015-15079-x.

[3] Z. Ye, J. Arrington, R.J. Hill, G. Lee, Phys. Lett. B 777 (2018) 8, https://doi.org/10.1016/j.physletb.2017.11.023.

[4] J.C. Bernauer, et al., A1 Collaboration, Phys. Rev. Lett. 105 (2010) 242001, https://doi.org/10.1103/PhysRevLett.105.242001.

[5] J.C. Bernauer, et al., A1 Collaboration, Phys. Rev. C 90 (1) (2014) 015206, https://doi.org/10.1103/PhysRevC.90.015206.

[6] M. Mihovilovič, et al., Phys. Lett. B 771 (2017) 194, https://doi.org/10.1016/j.physletb.2017.05.031.

[7] C.B. Crawford, et al., Phys. Rev. Lett. 98 (2007) 052301, https://doi.org/10.1103/PhysRevLett.98.052301.

[8] M. Paolone, et al., Phys. Rev. Lett. 105 (2010) 072001, https://doi.org/10.1103/PhysRevLett.105.072001.

[9] X. Zhan, et al., Phys. Lett. B 705 (2011) 59, https://doi.org/10.1016/j.physletb.2011.10.002.

[10] R. Pohl, et al., Nature 466 (2010) 213, https://doi.org/10.1038/nature09250.

[11] C.E. Carlson, Prog. Part. Nucl. Phys. 82 (2015) 59, https://doi.org/10.1016/j.ppnp.2015.01.002.

[12] J.J. Krauth, et al., arXiv:1706.00696 [physics.atom-ph].

[13] G. Hohler, E. Pietarinen, Phys. Lett. B 53 (1975) 471, https://doi.org/10.1016/0370-2693(75)90220-8.

[14] G. Hohler, et al., Nucl. Phys. B 114 (1976) 505, https://doi.org/10.1016/0550-3213(76)90449-1.

[15] M.A. Belushkin, H.-W. Hammer, U.-G. Meißner, Phys. Rev. C 75 (2007) 035202, https://doi.org/10.1103/PhysRevC.75.035202.

[16] I.T. Lorenz, H.-W. Hammer, U.-G. Meißner, Eur. Phys. J. A 48 (2012) 151, https://doi.org/10.1140/epja/i2012-12151-1.

[17] J.M. Alarcón, C. Weiss, Phys. Rev. C 96 (5) (2017) 055206, https://doi.org/10.1103/PhysRevC.96.055206.

[18] J.M. Alarcón, C. Weiss, Phys. Rev. C 97 (5) (2018) 055203, https://doi.org/10.1103/PhysRevC.97.055203, arXiv:1710.06430 [hep-ph].

[19] W.R. Frazer, J.R. Fulco, Phys. Rev. 117 (1960) 1603, https://doi.org/10.1103/PhysRev.117.1603.

[20] W.R. Frazer, J.R. Fulco, Phys. Rev. 117 (1960) 1609, https://doi.org/10.1103/PhysRev.117.1609.

[21] V.P. Druzhinin, S.I. Eidelman, S.I. Serednyakov, E.P. Solodov, Rev. Mod. Phys. 83 (2011) 1545, https://doi.org/10.1103/RevModPhys.83.1545.

[22] J.M. Alarcon, J. Martin Camalich, J.A. Oller, Ann. Phys. 336 (2013) 413, https://doi.org/10.1016/j.aop.2013.06.001.

[23] C. Patrignani, et al., Particle Data Group, Chin. Phys. C 40 (10) (2016) 100001, https://doi.org/10.1088/1674-1137/40/10/100001, and 2017 update.

[24] M. Hoferichter, et al., Eur. Phys. J. A 52 (11) (2016) 331, https://doi.org/10.1140/epja/i2016-16331-7.

[25] Z. Epstein, G. Paz, J. Roy, Phys. Rev. D 90 (7) (2014) 074027, https://doi.org/10.1103/PhysRevD.90.074027.

[26] M.A. Belushkin, H.-W. Hammer, U.G. Meißner, Phys. Lett. B 633 (2006) 507, https://doi.org/10.1016/j.physletb.2005.12.053.

[27] C. Alexandrou, et al., Phys. Rev. D 96 (3) (2017) 034503, https://doi.org/10.1103/PhysRevD.96.034503.

[28] X. Yan, et al., arXiv:1803.01629 [nucl-ex].

[29] J.M. Alarcón, A.N. Hiller Blin, M.J. Vicente Vacas, C. Weiss, Nucl. Phys. A 964 (2017) 18, https://doi.org/10.1016/j.nuclphysa.2017.05.002.